

Detachment of Plasters in Masonry Buildings: Analysis by Acoustic Emission and Numerical Simulation [†]

Alessandro Grazzini ^{*}, Giuseppe Lacidogna, Silvio Valente and Federico Accornero

Department of Structural, Geotechnical and Building Engineering, Politecnico di Torino, 10129 Turin, Italy; giuseppe.lacidogna@polito.it (G.L.); silvio.valente@polito.it (S.V.); federico.accornero@polito.it (F.A.)

^{*} Correspondence: alessandro.grazzini@polito.it; Tel.: +39-011-090-5315

[†] Presented at the 18th International Conference on Experimental Mechanics (ICEM18), Brussels, Belgium, 1–5 July 2018.

Published: 9 July 2018

Abstract: An innovative laboratory procedure is described for testing the mechanical adhesion of new dehumidified mortars applied in the restoration works. A specific adherence test was carried out on composite specimens made by stone block and repair mortar. During the laboratory test the acoustic emission (AE) technique was employed, in order to estimate the amount of energy released from fracture propagation in the adherence surface between mortar and stone. A numerical simulation follows the experimental data. The evolution of detachment process of mortar in a coupled stone brick–mortar system was analysed by AE signals, which can improve the numerical model and predict the failure mode in the adhesion surface of repair plaster.

Keywords: historical masonry; acoustic emission; plaster detachment; repair mortar; laboratory test

1. Introduction

The frequent de-bonding crack that happens on historical plasters, because of rain infiltrations and damp capillary action, needs restoration works made by new repair mortars. The great variety of historical masonries requires preliminary tests to assess the structural compatibility of the dehumidified mortars [1]. A new experimental procedure, carried out at the Politecnico Laboratory, was useful to analysis the mechanical adhesion of new dehumidified mortars applied to historical masonry surfaces. Moreover this methodology was tested at the Sacro Monte di Varallo, an UNESCO heritage site in Italy [2], where the original plasters of historical chapels were damaged by rain infiltrations and freezing-thawing cycles that compromise the adhesion to masonries (Figure 1).

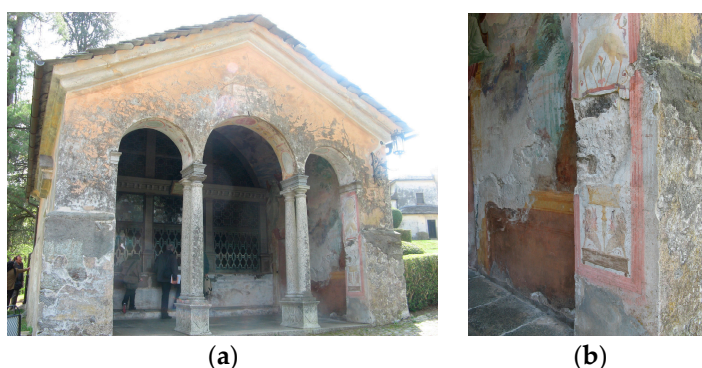


Figure 1. Chapel of the Temptations (a), and delamination problems of the historical plasters (b).

Sometime the mechanical incompatibility of applied repair mortars determined the detachment of new dehumidified plasters. Through shear static tests on stone-mortar composite specimens, it was possible to select the dehumidified mortar with greater durability guarantees. The Acoustic Emission (AE) monitoring technique was employed during static tests for assessing damage evolution inside the adherence surface [3].

2. Materials and Method

A specific geometry of composite specimens was devised in order to test the adherence between a chosen repair mortar and a stone block. The hydraulic lime mortar was a pre-blended transpiring product, useful for historical masonry damaged by dampness. Every mixed specimen was made by means of mortar layers applied to both shorter faces of the stone brick (Figure 2). In this way, a plaster layer applied to stone masonry was occurred. The Young’s modulus of repair mortar was 7000 MPa, the compressive strength was 33.8 MPa.

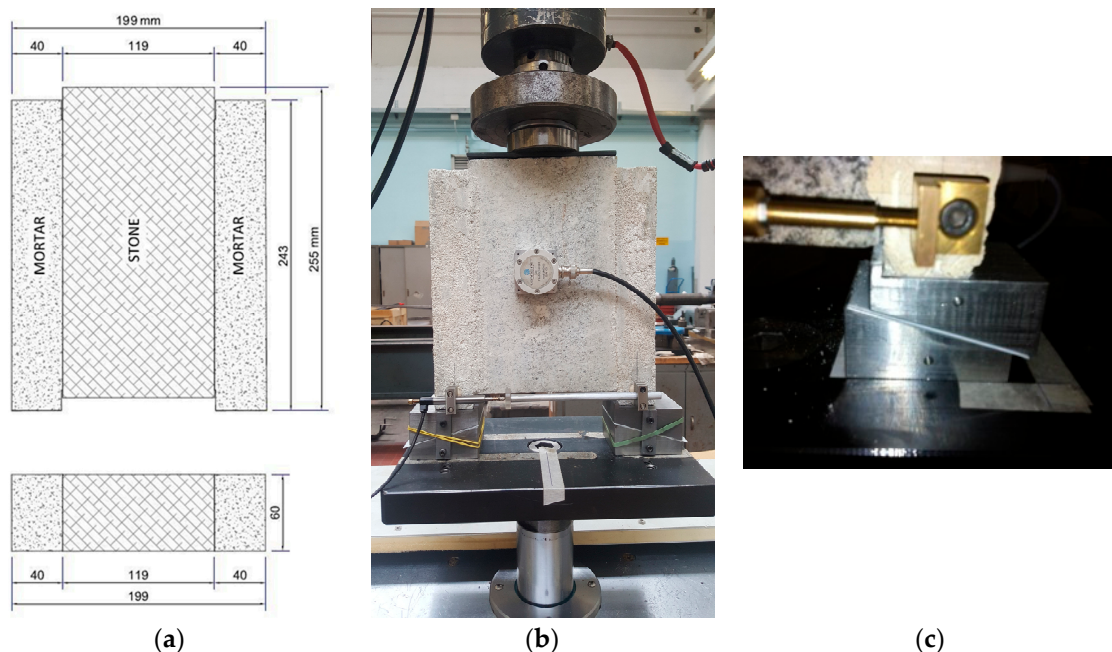


Figure 2. Geometry of composite specimen (a); test setup (b); wedges’ geometry (c).

The adhesion of mortar layers applied to stone surface was facilitate by a picket work through a drill, in order to simulate the real discontinuities on the wall surface that favor the adhesion of the plaster. At the bottom and at the top of the specimens two symmetrical discontinuities were made, as showed in Figure 2b. These notches favored the propagation of multiple cracks, and tested the adhesion of materials. An inductive horizontal displacement transducer was applied at the bottom of the specimen (Figure 2). The vertical displacements were recorded by the piston’s stroke of the 250 kN servo controlled machine. The shear tests were carried out through monotonous compression load by controlling the horizontal opening. Static tests have been performed after 28 days of maturation. The mortar layers rested on a double system of steel wedges, as showed in Figure 2c. The steel wedges were coupled by a Teflon layer thick 1 mm in order to for reduce the horizontal friction. The “SM” (Stone brick-Mortar) label has been associated with each specimen with its sequence number.

3. Results of the Acoustic Emission Monitoring

The estimation and classification of active cracks is a great deal of the AE technique, and in general for Non-destructive monitoring techniques [4]. AE signals due to microcracks were detected by AE sensors attached on the specimen’s surface by a silicon glue. The signal waveforms were

recorded by the AE measurement system. The AE waves were amplified with 60 dB gain before they have been processed, setting the acquisition threshold level up to 2 mV.

In order to classify active cracks, the AE signals parameters, such as rise time and peak amplitude, were considered to calculate the rise angle (RA) value, defined as the ratio of the rise time (expressed in ms) to the peak amplitude (expressed in V). The shape of the AE waveforms is typical of the fracture mode. Shear events are characterized by long rise times and usually high amplitudes, whereas low rise time values are typical of tensile crack propagations. These conditions are synthesized by the RA value [4]. Another parameter used to characterize the cracking mode is the Average Frequency (AF) expressed in kHz. In general, the shift from higher to lower values of AF could indicate the shift of the cracking mode from tensile to shear [4]. Nevertheless, when a cracking process involves the opening of large cracks (Mode I), the frequency attenuation must be a function of this discontinuity. In other words, in this case the wavelength of the AE signals needs to be larger for the crack opening to be overcome, and the shift of the frequencies from higher to lower values could support also a dominant tensile cracking mode.

Briefly, the results of the AE monitoring are presented only for specimen SM4. The load vs. time diagram of the specimen SM4, together with AE cumulated curve and AE rate, is shown in Figure 3a. During the first part of the test, when the load increases proportionally over time, there are few AE signals. However, a clear growth in the AE hits is obtained in the correspondence of each sharply decrease of the load vs. time curve. This supports the fact that the AE signals are mainly associated with the energy emitted by the specimen during the delamination of the mortar from the stone block (snap-back instabilities). All the AE signals detected, about 180 hits, are represented in Figure 3a. However, most of these hits are characterized by a random oscillatory appearance, which results from the overlapping of multiple burst type signals of undistinguished amplitudes. This is due to the very brittle behavior of the delamination process, which generated many signals overlaps. On the other hand, all the AE signals obtained during the test, proving a clear dominating average frequency, and a sharp peak in the voltage are shown in Figure 3b and used to find AF and RA values. The dominating frequency has been calculated by using the FFT (Fast Fourier Transform).

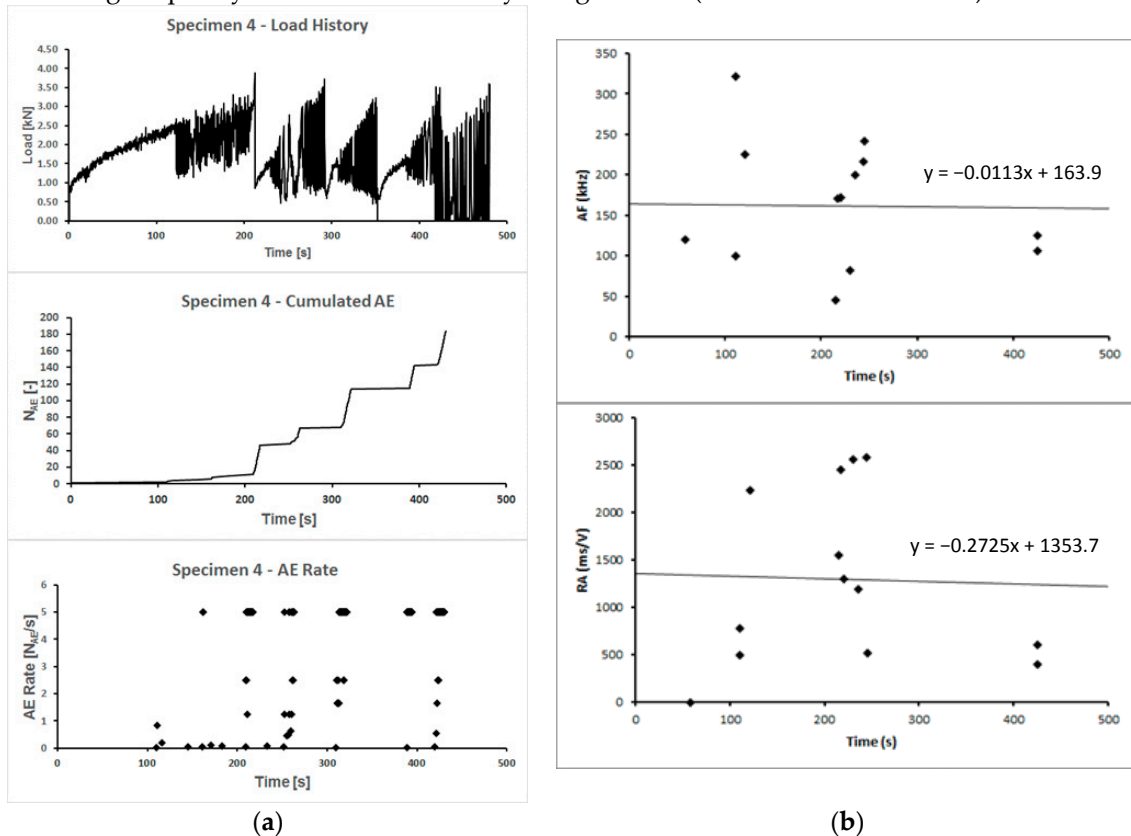


Figure 3. Diagram vs time of SM4: Load, Cumulated AE, and AE rate (a); Average Frequency AF and Rise Angle RA (b).

Using the ordinary least squares method, the linear regression of the signal frequencies (AF) and the signals rise angles (RA) were traced during the whole test, as showed in Figure 3b. Considerable variations from the mean trend were observed in particular immediately after 100 s from the beginning of the test, around 200 s, and around 420 s towards the end of the test. In the first phase, from 0 to 120 s, rise angles with low values prevail, while the frequencies are oscillating with the higher values more distant from the average trend. This indicates a prevalent Mode I in the delamination process in the initial loading phase. In the second phase, the highest values of the RAs during the whole test were obtained, while the frequencies continue to oscillate with the lowest values more distant from the average. This behavior shows how the delamination process that leads to collapse develops with sudden stress drops and is mainly accompanied by the sliding of the mortar with respect to the stone block (Mode II). In the final phase, over 400 s, the frequencies are still lowered below the average line, while the RAs once again become low, so it can be said that there is no prevailing fracture mode before the specimen collapses definitively.

4. Numerical Simulation

The Barenblatt–Dugdale–Hillerborg model, also known as the cohesive crack model, is a good numerical approach to simulate the behaviour of quasi-brittle materials, as the stone-mortar delamination. The crack initiation criterion is assumed as:

$$\left(\frac{\sigma_0}{f_t}\right)^2 + \left(\frac{\tau_0}{f_s}\right)^2 = 1 \tag{1}$$

where σ_0 and τ_0 are the stresses respectively orthogonal and tangential directions, f_t and f_s are the respective strengths. The fictional crack tip is the point where Equation (1) is proved. The cohesive stresses present on the non-linear fracture process zone (FPZ) are decreasing functions of the effective value of the displacement discontinuity w_{eff} [5–9]. It was assumed:

$$w_{\text{eff}} = \sqrt{\left(\frac{w_n}{w_{\text{nc}}}\right)^2 + \left(\frac{w_t}{w_{\text{tc}}}\right)^2} \tag{2}$$

where w_n is the first component of the mutual-orthogonal displacement, and w_t is the second one (tangential to the interface); the related critical values are w_{nc} and w_{tc} . If $w_{\text{eff}} > 1$ there is no stress transfer and the crack is stress free; otherwise, the stresses are decreasing functions of w_{eff} that follow a pre-defined softening law. The above mentioned law is assumed:

$$\frac{\sigma}{\sigma_0} = \frac{\tau}{\tau_0} = \left[1 - \frac{1 - \exp(-\alpha \cdot w_{\text{eff}})}{1 - \exp(-\alpha)}\right] \tag{3}$$

where $\alpha = 5$ is assumed. Real crack tip is called the point where $w_{\text{eff}} = 1$. Outside the FPZ the material had a linear-elastic behavior. The fracture process starts symmetrically, but loses this property afterwards [10–12] because of the propagation of the round-off errors. In this case the numerical simulation was controlled according a uniform downward velocity to the upper edge on the rock. This choice was able to prevent the growth of the round-off errors so that, from an engineering point of view, the propagation of the two cohesive cracks occurs symmetrically. The interface strength properties were assumed as shown in Tables 1 and 2. The numerical analyses were performed using the ABAQUS code. Figure 4 shows the deformed mesh of finite element model.

Table 1. The interface strength properties.

f_t (N/mm ²)	f_s (N/mm ²)	w_{nc} (mm)	w_{tc} (mm)
0.8	1.0	0.015	0.015

Table 2. Mechanical characteristics of materials.

	E (N/mm ²)	ν
Mortar	7000	0.15
Rock	35,000	0.20

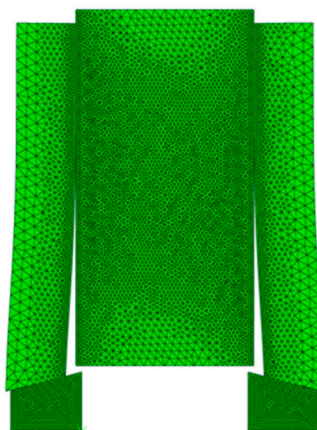


Figure 4. Finite element deformation during max displacement.

5. Discussion

The notch tips tested the adherence between the repair plaster and masonry stone. The experimental procedure was able to simulate the fatigue stresses that can lead to de-bonding of a dehumidified plaster. Four stress singularity points were in the stone-mortar specimens: two notch tips at the top, and two at the bottom. These are the weakest points involved in the singular stress fields. The cracks beginning from the bottom were faster than the cracks from the top, because of the wedges. The friction, reduced by the Teflon sheet, is not taken into account in the numerical simulation and the materials are considered homogeneous. This is the reason why the response curve is continuous (Figure 5). On the contrary, the properties of the rock specimen can change from point to point. This is the reason why the experimental curve shows many discontinuities. The numerical model represents an ideal behaviour which, in particular in the early stages of loading, fit the average values of the experimental curves, but it is not able to identify the snap-back instabilities that experimentally occur during the delamination process.

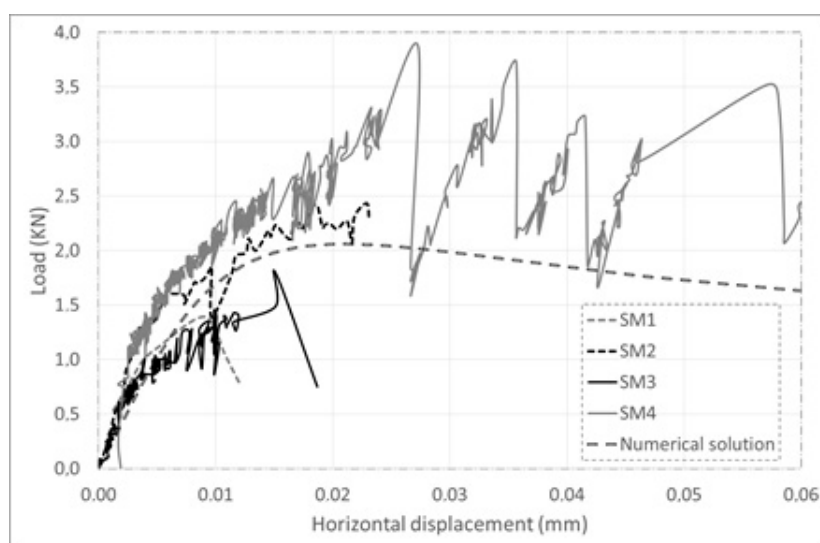


Figure 5. Load—horizontal displacement curves of the specimens vs. the numerical solution.

6. Conclusions

To evaluate the durability of restoration interventions it is very important to test the materials to be used before their application. The selection of the most durable dehumidified mortar is essential in order to avoid de-bonding processes due to hygrometric actions. The experimental procedure allowed to test the adherence between the repair plaster and the historical masonry stone, and to produce, in a static test, the interface stresses that can be also caused by freeze and thaw actions.

The AE results obtained from the compression tests on the SM4 sample prove that the AE signals are prevalent associated with the energy emitted by the specimen during the mortar delamination from the stone block. Moreover, the variation of the AE parameters during the loading process strictly depends on the evolution of crack mode. The lower RA values indicate more tensile nature of fracture events. From the obtained results it was possible to identify a prevalent Mode I in the delamination process during the initial loading phases. The delamination process was then carried out with sudden load drops, mainly accompanied by the sliding of the mortar with respect to the stone block (Mode II). While, in the final loading phase, no prevalent fracture mode emerged before the specimen definitively collapses. The non-linear phenomena that occurs at the interface between mortar and stone during the de-bonding process were theoretically interpret through the cohesive crack model.

Author Contributions: A.G. and S.V. conceived and designed the experiments; F.A. performed the experiments; G.L. and F.A. analyzed the AE data; S.V. contributed numerical analysis; A.G., G.L. and S.V. wrote the paper.

Conflicts of Interest: The authors declare no conflict of interest.

References

1. Bocca, P.; Grazzini, A. Mechanical properties and freezing-thawing durability of strengthening mortars. *J. Mater. Civ. Eng.* **2013**, *25*, 274–280, doi:10.1061/(ASCE)MT.1943-5533.0000597.
2. Bocca, P.; Valente, S.; Grazzini, A.; Alberto, A. Detachment analysis of dehumidified repair mortars applied to historical masonry walls. *Int. J. Archit. Herit.* **2014**, *8*, 336–348, doi:10.1080/15583058.2013.826304.
3. Carpinteri, A.; Grazzini, A.; Lacidogna, G.; Manuello, A. Durability evaluation of reinforced masonry by fatigue tests and acoustic emission technique. *Struct. Control Health Monit.* **2014**, *21*, 950–961, doi:10.1002/stc.1623.
4. Carpinteri, A.; Lacidogna, G.; Accornero, F.; Mpalaskas, F.; Matikas, A.; Aggelis, D. Influence of damage in the Acoustic Emission parameters. *Cem. Concr. Compos.* **2013**, *44*, 9–16, doi:10.1016/j.cemconcomp.2013.08.001.
5. Barpi, F.; Valente, S. The cohesive frictional crack model applied to the analysis of the dam-foundation joint. *Eng. Fract. Mech.* **2010**, *77*, 2182–2191, doi:10.1016/j.engfracmech.2010.02.030.
6. Barpi, F.; Valente, S. Fuzzy parameters analysis of time-dependent fracture of concrete dam models. *Int. J. Numer. Anal. Methods Geomech.* **2002**, *26*, 1005–1027, doi:10.1002/nag.235.
7. Barpi, F.; Valente, S. A fractional order rate approach for modeling concrete structures subjected to creep and fracture. *Int. J. Solids Struct.* **2004**, *41*, 2607–2621, doi:10.1016/j.ijsolstr.2003.12.025.
8. Barpi, F.; Valente, S. Lifetime evaluation of concrete structures under sustained post-peak loading. *Eng. Fract. Mech.* **2005**, *72*, 2427–2443, doi:10.1016/j.engfracmech.2005.03.010.
9. Barpi, F.; Valente, S. Modeling water penetration at dam-foundation joint. *Eng. Fract. Mech.* **2008**, *75*, 629–642, doi:10.1016/j.engfracmech.2007.02.008.
10. Barpi, F.; Valente, S. Size-effects induced bifurcation phenomena during multiple cohesive crack propagation. *Int. J. Solids Struct.* **1998**, *35*, 1851–1861, doi:10.1016/S0020-7683(97)00158-3.

11. Alberto, A.; Antonaci, P.; Valente, S. Damage analysis of brick-to-mortar interfaces. In Proceedings of the 11th International Conference on the Mechanical Behavior of Materials, Lake Como, Italy, 5–9 June 2011; Elsevier: New York, NY, USA, 2011; pp. 1151–1156.
12. Bocca, P.; Grazzini, A.; Masera, D.; Alberto, A.; Valente, S. Mechanical interaction between historical brick and repair mortar: Experimental and numerical tests. *J. Phys. Conf. Ser.* **2011**, *305*, 012126, doi:10.1088/1742-6596/305/1/012126.



© 2018 by the authors. Licensee MDPI, Basel, Switzerland. This article is an open access article distributed under the terms and conditions of the Creative Commons Attribution (CC BY) license (<http://creativecommons.org/licenses/by/4.0/>).